Deficient endoplasmic reticulum-mitochondrial phosphatidylserine transfer causes liver disease

María Isabel Hernández-Alvarez[1,3,11*], David Sebastián[1,2,3], Sara Vives [1], Saška Ivanova[1,2,3], Paola Bartoccioni[1,2,4], Pamela Kakimoto [1], Natalia Plana[1], Sónia R. Veiga[5], Vanessa Hernández[1], Nuno Vasconcelos[1], Peddinti Gopalacharyulu[6], Anna Adrover[1], Mariona Jové [13], Reinald Pamplona [13], Antonio Berenguer-Llergo[1], Isabel Gordaliza[1,2,3], Enrique Calvo[11],Noemí Cabré[12], Rui Castro[7], Antonija Kuzmanic [1], Marie Boutant[8], David Sala[1,2,3], Tuulia Hyotylainen[9], Matej Orešič[10], Joana Fort[1,2,4], Ekaitz Errasti-Murugarren[1,4], Modesto Orozco [1],Jorge Joven[12], Carles Cantó[8], Manuel Palacin[1,2,4], Sonia Fernández-Veledo[3,11], Joan Vendrell[3,11] and Antonio Zorzano[1,2,3*]

[1]Institute for Research in Biomedicine (IRB Barcelona). The Barcelona Institute of Science and Technology, Barcelona, Spain;

[2]Departament de Bioquímica i Biomedicina Molecular, Facultat de Biologia, 08028 Barcelona, Spain;

[3]CIBER de Diabetes y Enfermedades Metabólicas Asociadas (CIBERDEM), Instituto de Salud Carlos III;

[4]CIBERER, Instituto de Salud Carlos III, Spain;

[5] Cancer Metabolism Group, ONCOBELL Program, Bellvitge Biomedical Research Institute (IDIBELL), Barcelona, Spain;

[6]Institute for Molecular Medicine Finland (FIMM) Nordic EMBL Partnership for Molecular Medicine Biomedicum, University of Helsinki Finland;

[7]Research Institute for Medicines (iMed.ULisboa), and Department of Biochemistry and Human Biology, Faculty of Pharmacy, Universidade de Lisboa, 1649-003 Lisboa, Portugal;

[8]Nestlé Institute of Health Sciences SA, Lausanne (Switzerland);

[9]Department of Chemistry, University of Örebro, Örebro, Sweden;

[10]Turku Centre for Biotechnology, University of Turku and Åbo Akademi University, Turku, Finland;

[11]Hospital Universitari de Tarragona Joan XXIII, Institut Investigació Sanitaria Pere Virgili, Universitat Rovira i Virgili, Tarragona, Spain.

[12]Biochemical Research Unit, Hospital Universitari de Sant Joan, Institut d'Investigació Sanitària Pere Virgili, Universitat Rovira i Virgili, C. Sant Joan s/n, Reus, 43201, Spain

*Corresponding author. Institute for Research in Biomedicine, C/ Baldiri Reixac 10, 08028 Barcelona. Tel:+34-934037197; Fax:+34-934034717; E-mail: antonio.zorzano@irbbarcelona.org; misabel.hernandez.alvarez@gmail.com

The authors declare no conflict of interest. CC and MB are employees of the Nestlé Institute of Health Sciences S.A.

Summary

Non-alcoholic fatty liver disease is the most common liver disease worldwide. Here, we show that the mitochondrial protein mitofusin 2 (Mfn2) protects against liver disease. Reduced Mfn2 expression was detected in liver biopsies from patients with non-alcoholic steatohepatitis (NASH). Moreover, reduced Mfn2 expression was detected in mouse models of steatosis or NASH, and its re-expression in a NASH mouse model ameliorated the disease. Liver-specific ablation of Mfn2 in mice provoked inflammation, triglyceride accumulation, fibrosis and liver cancer. We demonstrate that Mfn2 binds phosphatidylserine (PS) and can specifically extract PS into membrane domains, favoring PS transfer to mitochondria, as well as mitochondrial phosphatidylethanolamine (PE) synthesis. Consequently, hepatic Mfn2 deficiency reduces PS transfer and phospholipid synthesis, leading to endoplasmic reticulum (ER) stress and the development of a NASH-like phenotype and liver cancer. Thus, ablation of Mfn2 in liver reveals that disruption of ER-mitochondrial PS transfer is a new mechanism involved in the development of liver disease.

Introduction

Non-alcoholic fatty liver disease (NAFLD) is among the most common liver diseases worldwide, with increasing prevalence in parallel with the obesity/metabolic syndrome epidemic. NAFLD represents a clinical spectrum ranging from simple steatosis and non-alcoholic steatohepatitis (NASH) to cirrhosis and hepatocellular carcinoma (HCC)[1]. NASH is accompanied by inflammation, cell death, and fibrosis, and is characterized histologically by the presence of ballooning hepatocytes and lobular inflammation with or without perisinusoidal fibrosis and steatosis[2]. Hepatic inflammation is a complex process that originates in response to a variety of stress conditions[3]. In the course of the inflammatory process, liver hepatocytes frequently die by programmed cell death. The persistent cycle of "necro-inflammation" and hepatocyte regeneration is believed to enhance the risk of genetic mutation in hepatocytes, promoting survival and expansion of initiated cells. The result is increased cell growth, also referred to as compensatory proliferation, which can lead to tumor development[4,5]. In this context, epidemiological and clinical studies have provided convincing evidence that chronic inflammation leads to carcinogenesis[6-9].

Several potential factors influencing NASH progression are known to interact[10-15], such as hepatic endoplasmic reticulum (ER) stress, oxidative stress, mitochondrial dysfunction and lipotoxicity. Mitochondrial function is governed by the preservation of a normal lipid composition[16-19], which is dependent on the capacity of mitochondria to synthesize phospholipids, and by the traffic of lipids from the ER to mitochondria[20-22]. Specifically, phosphatidylserine (PS) is primarily synthesized in the ER and is imported into mitochondria by transient membrane contact between mitochondria-associated ER membranes (MAMs) and the mitochondrial outer membrane[23]. In mitochondria, PS is converted into phosphatidylethanolamine (PE), which is then imported into the ER for conversion to phosphatidylcholine (PC)[16,21,24,25]. Accordingly, MAMs are key sites for synthesis and traffic of phospholipids[17,25].

Mitofusin 2 (Mfn2) is a mitochondrial membrane protein with a role connecting ER membranes to mitochondria[26-28], and its depletion causes ER stress[29-31]. Mfn2 plays a relevant role in the maintenance of mitochondrial metabolism, insulin signaling and energy homeostasis[30-33]. Cancer cells of different origin show a low expression of Mfn2 [34-37]. In addition, Mfn2 levels are significantly downregulated in HCC tissue compared

with corresponding adjacent normal tissue, and there is a negative correlation between Mfn2 levels and the prognosis of cancer[38-40]. Mfn2 overexpression in hepatocellular carcinoma or colorectal cancer cells reduces cell proliferation and induces spontaneous apoptosis[35,37]. However, it is unknown whether Mfn2 downregulation is a cause or a consequence of cancer, and in addition, there are no data linking Mfn2 to NALFD progression.

Here we show that hepatic Mfn2 is downregulated both in patients with NASH, and in subjects borderline for NASH. Further, mouse models of hepatic lipid accumulation or NASH present lower levels of Mfn2 in liver, and the re-expression of Mfn2 in liver ameliorates the NASH phenotype. We also demonstrate that hepatic Mfn2 ablation causes a NASH-like phenotype that progresses to liver cancer with age. We show that Mfn2 binds to and participates in the transfer of PS. Accordingly, hepatic Mfn2 deficiency causes a reduced transfer of PS from ER to mitochondria, which leads to reduced PS synthesis and ER stress, in turn causing inflammation, fibrosis and liver cancer. Overall, our data strongly suggest that Mfn2 constitutes a new target for the treatment of NALFD.

Results

Human liver samples of non-alcoholic steatohepatitis present low levels of Mfn2

To investigate whether Mfn2 is dysregulated in NASH, we compared its expression in liver biopsies from patients with steatosis or NASH. Clinical, anthropometric, and biochemical data of this cohort have been reported previously[41]. Results showed that protein levels of Mfn2 were significantly lower in liver from patients with NASH than in subjects with simple steatosis (Figure 1A). We also analyzed human liver biopsies from a second cohort of subjects without NASH (NAS index $\leq$3) and close to borderline NASH (NAS index $\geq$5). NAS scoring was performed according Takeda et al.,[42]. Clinical characteristics of these patients are shown in Supplementary Table 1. Both Mfn2 mRNA and protein levels were significantly decreased in patients with borderline NASH (Figures S1A, S1B and S1C). By contrast, expression of the Mfn2 homologue Mfn1 was unaltered in this group (Figure S1D). Overall, these data show that Mfn2 is down-regulated in human liver during progression from steatosis to NASH.

Mouse models of non-alcoholic liver disease have low hepatic levels of Mfn2

To document the possible involvement of Mfn2 in NALFD, we studied its expression in C57BL6/J mice with steatosis induced by high-fat diet (HFD) over three weeks, a time sufficient to trigger hepatic steatosis[43]. Mfn2 protein expression in liver was significanly lower in the HFD group than in the control group (Figures 1B, and S1E). Because mice on HFD show fatty liver and obesity but not fibrosis[44], we utilized a well-established mouse model of NASH consisting of a methionine/choline-deficient diet combined with 45% HFD and supplemented with 0.1% L-methionine in drinking water, to avoid weight loss[44] (hereafter termed MCD). C57BL6/J mice on MCD diet for 3 weeks showed substantial fat accumulation and liver fibrosis (detected by H&E and Sirius Red staining, respectively) (Figure 1C). Further, liver triglyceride levels and mRNA levels of inflammatory markers and the fibrotic marker TGFβ were significantly higher in mice on MCD diet than on control diet (Figures 1D, S1F and S1G). Under these conditions Mfn2 levels were diminished (Figures 1E, and S1H), and this decrease was greater in mice on MCD diet than on HFD (Figure 1B and 1E). Consistent with the data in human biopsies, Mfn1 protein levels were unaltered in mice on MCD diet (Figure

S1I). These results are consistent with a specific progressive repression of Mfn2 in mouse liver disease.

Mfn2 ablation causes chronic hepatic inflammation and abnormal lipid metabolism

To substantiate the role of Mfn2 in liver as a trigger of the NASH-like phenotype, we analyzed liver-specific Mfn2 knockout mice (L-KO) generated in our laboratory[31]. Under normal chow diet, 8 week-old L-KO mice showed a significant increase in the abundance of hepatic and plasma pro-inflammatory cytokines (Figures 1F, S2A and S2B), expression of hepatic pro-inflammatory genes (Figure S2C) and a modest but significant accumulation of triglycerides (Figure 1G). This occurred in the absence of changes in body weight, food intake or circulating lipids (Figures S2D–H). Further analysis of lipid metabolism in hepatocytes isolated from L-KO and control mice revealed that the esterification of oleate into diacylglycerol and triacylglycerol was enhanced in the former, but their incorporation into phospholipids was decreased (Figure 1H). Under these conditions, oleate β-oxidation was decreased in Mfn2-deficient hepatocytes (Figure S2I). Further, the expression of *de novo* lipogenesis and esterification genes was modestly elevated in liver from L-KO mice (Figures S2J). In sum, L-KO mice show a pattern typical of disturbances in hepatic lipid metabolism.

Mfn2 ablation causes apoptosis, increased cell growth, fibrosis and liver cancer

It is known that chronic hepatic inflammation is associated with enhanced apoptosis, leading to compensatory cell proliferation and fibrosis, which are known risk factors for liver cancer[45,46]. Given the chronic inflammation detected in L-KO mice, we analyzed the development of these processes to determine whether Mfn2 deficiency leads to liver cancer progression. Under normal conditions, apoptosis was higher in liver from L-KO mice than from controls, as demonstrated by increased levels of cleaved PARP-1 and cleaved caspase-3 (Figures S3A and S3B), and was accompanied by a higher number of Ki67-positive cells (Figure S3C), indicating enhanced proliferation. Furthermore, the expression of genes encoding fibrotic markers was also elevated in L-KO livers (Figure 1J), and Sirius red staining and transmission electron microscopy revealed a marked accumulation of extracellular collagen in livers at 27 weeks of age (Figure 1I).

We next explored whether hepatic Mfn2 deficiency promotes liver cancer as a consequence of the natural progression of liver disease. Accordingly, L-KO and control mice on normal diet were examined for liver tumors at twenty-four months of age. Analysis showed that the number of tumors was significantly higher in L-KO mice than in control mice, and tumor volume was also greater (Figures 1K and S3D). We next sought to validate these results by investigating whether L-KO mice showed a differential predisposition to the liver-specific carcinogen diethylnitrosamine (DEN). Treatment of mice with DEN triggers a well-known cascade of events in liver that include DNA damage and apoptosis of centrilobular hepatocytes, production of proinflammatory cytokines and compensatory proliferation[47]. As a first approach, we induced liver DNA damage with a single high-dose intraperitoneal injection of DEN (50 mg/kg) to assess the acute liver response. Immunohistological examination of livers 48 h after DEN injection revealed a stronger DNA damage response in centrilobular regions in L-KO mice than in controls, and this accompanied by greater levels of compensatory proliferation (Figures S3E, S3F, and S3G). We next treated control and L-KO mice with a single lower dose of DEN (5 mg/kg), followed by continued exposure to HFD. After seven months L-KO mice subjected to DEN-HFD treatment showed a larger number of tumors and greater tumor size compared to control treated mice (Figure S3H). Thus, our data indicate that hepatic Mfn2 ablation leads to apoptosis, increased cell proliferation, fibrosis, and a greater susceptibility to develop liver cancer.

Mfn2 re-expression restores normal liver metabolism in L-KO mice

To assess whether the alterations detected in Mfn2-deficient livers were attributable to Mfn2 loss-of-function or to compensatory mechanisms, we re-expressed Mfn2 in L-KO mice by intravenous administration of adenoviruses encoding either Mfn2 or LacZ (AdC, used as a control). Upon Mfn2 re-expression (Figure S4A) hepatic and plasma cytokines returned to control levels (Figures S4B–D) and the expression of fibrosis genes and pro-inflammatory genes were markedly down-regulated (Figure S4E and S4G). Moreover, triacylglycerol levels were normalized (Figure S4F), and oleate β-oxidation was enhanced (Figure S4H).

We have previously reported that under normal chow diet, 8-week-old L-KO mice present an elevated unfolded protein response (UPR)[31]. Thus, we surveyed the impact of Mfn2 re-expression on ER stress markers. Results showed that Mfn2 re-expression normalized the different UPR parameters (Figure S4I). These data strongly suggest that Mfn2 is directly responsible for the liver abnormalities found in L-KO mice.

Normalization of ER stress triggered by Mfn2 deficiency ameliorates inflammation and fibrosis but not the impaired lipid metabolism

The up-regulation of UPR proteins, such as CHOP, is sufficient to promote liver apoptosis, inflammation, compensatory proliferation, fibrosis and liver cancer[48]. To begin to elucidate the mechanisms by which Mfn2 deficiency triggers the development of cancer, we examined the contribution of ER stress to these processes in the L-KO model. We blocked ER stress by overexpressing a critical regulator of UPR signaling, BIP (GRP-78). Because hepatic BIP gain-of-function in control mice has been shown to cause hypoglycemia and sudden death, even upon administration of very low levels of adenovirus, in models that do not present UPR activation (data not shown and previous reports[49,50]), we expressed BIP by adenoviral intravenous injection only in L-KO mice, which show chronic ER stress.

Acute BIP overexpression decreased UPR signaling in L-KO mice (Figure 2A, and S5A). Moreover, liver and plasma circulating pro-inflammatory cytokines were normalized by BIP (Figure 2B, and 2C), and the expression of genes encoding pro-inflammatory or fibrotic factors was also markedly lower than that seen in equivalent controls (Figure 2D and S5B). Similarly, apoptosis and cell proliferation were decreased in L-KO mice expressing BIP (Figure S5C–D). In the context of mitochondrial metabolism, BIP expression enhanced oleate oxidation (Figure S5E) and reduced ROS production measured as hydrogen peroxide (Figure S5F), thereby recovering mitochondrial function, which is in keeping with our previous data[29]. Intriguingly, BIP overexpression failed to restore hepatic triglyceride levels (Figure 2E) or the incorporation of oleate into lipids (Figure 2F). These data indicate that the hepatic mitochondrial dysfunction, inflammation, fibrosis, apoptosis and increased proliferation detected in L-KO mice lies downstream of ER stress and UPR signaling.

Mfn2 plays a crucial role in hepatic phospholipid metabolism

It has been reported that an aberrant phospholipid composition of the ER membrane is a potent activator of the UPR[51-53]. Accordingly, we studied the total hepatic phospholipid content in L-KO mice in an attempt to identify mechanisms linking Mfn2 deficiency and UPR. Results from lipidomics analysis showed that L-KO mice had a decreased abundance of total hepatic PE and PC species (Figure 3A; statistical significance of the data is shown in Supplementary Table 2). Consistent with these data, the lipidomics profile of hepatic MAMs and mitochondrial fractions from L-KO and control mice was different (Figures S6A, and S6D), with a decrease in the abundance of PE and PC species in the former (Figures S6B, S6C, S6E, and SEF; Supplementary Table 3). Because Mfn2 and some proteins of hepatic phospholipid synthesis are localized in mitochondria-ER contact sites (schematic shown in Figure 3B)[26,29,54,55], we monitored the incorporation of radiolabeled L-serine (L-Ser) into PS, PE, and PC in hepatic MAM fractions from control and L-KO mice. We found that this incorporation was significantly decreased in MAM fractions from L-KO mice (Figure 3C–E).

We next questioned whether ER stress plays a role in the defects detected in phospholipid synthesis by analyzing BIP-expressing L-KO mice. BIP expression failed to improve the incorporation of L-Ser into PS, PE or PC (Figure 3F); however, re-expression of Mfn2 completely rescued L-Ser incorporation into phospholipids (Figure 3G). Overall, our data indicate that hepatic Mfn2 depletion alters phospholipid synthesis and that these effects are not a consequence of ER stress.

Phospholipid metabolism in mammalian cells depends on the activity of many enzymes including phosphatidylserine synthase 1 (PSS1), phosphatidylserine synthase 2 (PSS2), and PE N-methyltransferase (PEMT), which are localized in MAMs and the ER; and PS decarboxylase (PISD), which is found in mitochondria[20,21]. We therefore analyzed whether loss of Mfn2 altered the expression of these proteins. Analysis by western blotting showed that the hepatic expression of PSS1 and PSS2 proteins was significantly lower in L-KO mice than in control mice (Figure 3H), whereas no changes were observed for PEMT (Figure S6G) or PISD (data not shown).

We next assessed the protein composition in MAMs by examining the abundance of MAM-enriched proteins in liver upon subcellular fractionation (Figure 3I and S6H). Western blotting of hepatic MAM fractions revealed a 50% reduction in PSS1 expression in L-KO mice (Figure 3I), whereas no changes were found for PSS2 whose expression was barely detectable (Figure 3I, and Figure S6I). Moreover, levels of PACS-2, Sig1R, and calnexin were elevated in MAMs from L-KO mice (Figures 3I, S6H, and S6I), which resembles the alterations in MAM composition in models of insulin resistance and aberrant lipid metabolism[52,56]. Thus, our results suggest that Mfn2 regulates phospholipid biosynthesis through PSS1 and PSS2 protein levels.

Alterations of lipid metabolism in L-KO mice are independent of the distance between ER and mitochondria

Given the role of Mfn2 in tethering ER to mitochondria [26-28], we explored whether the distance between mitochondria and ER might regulate phospholipid synthesis in Mfn2-ablated conditions. To do this, we used a recombinant adenovirus construct encoding a synthetic linker (RFP-linker) that increases the number ER-mitochondria contact sites, thus forcing ER-mitochondria interactions in L-KO mice (Figure S7A). Western blot analysis of RFP expression confirmed the expression of the linker (Figure S7A). L-KO mice expressing this linker showed a normalization of L-Ser incorporation into PS (Figure S7B); however, it failed to correct the synthesis of PE or PC, hepatic triacylglyceride levels, ER stress or PSS1 expression (Figures S7B–S7F). Under these conditions, PSS2 abundance was actually enhanced in L-KO mice (Figure S7F), which may explain the normalization of PS synthesis (Figure S7B). These results indicate that altered ER-mitochondria contact does not explain the lower synthesis of PE and PC in MAMs of Mfn2-deficient livers.

Down-regulation of hepatic PSS1/2 phenocopies Mfn2 ablation

In light of the above findings, we hypothesized that a decrease in phospholipid synthesis in MAMs causes hepatic triglyceride accumulation and ER stress in liver. To test this, we induced downregulation of either PSS1 or PSS2 in wild-type mice. Silencing of PSS1 by intravenous injection of a specific shRNA adenovirus caused the upregulation

of hepatic PSS2 and *vice versa* (Figure S8A,B), observations that are in agreement with previous data[57-61]. On the basis of these findings, which point to a strong adaptation process, we silenced both PSS1 and PSS2 in wild-type mice using two specific shRNA adenoviruses, which decreased the hepatic expression of both proteins by ~90% (Figure 4A and S8C). Analysis of hepatic MAM fractions showed a significant decrease of PSS1 in PSS1/2 knockdown (hereafter termed KD) mice (Figure 4B). This resulted in a decrease in the incorporation of L-Ser into PS and PE (Figure 4C) and an increase in hepatic triacylglycerol and oleate incorporation into lipids (Figure 4D and S8D). KD mice also showed ER stress (Figure 4E and S8E), and a higher expression of the fibrosis gene α-SMA and pro-inflammatory genes in liver (Figure 4F and S8F). In keeping with these observations, levels of hepatic pro-inflammatory cytokines were elevated in KD livers (Figure S8G); however, mitochondrial function (oleate oxidation or liver hydrogen peroxide production) was unaltered (Figure S8H and S8I).

Analysis of MAM protein composition revealed alterations in response to hepatic PSS1/2 silencing, with a significant decrease of Mfn2 expression in KD mice (Figure 4G). Also, PACS-2, Sig1R, and calnexin proteins were more abundant in MAMs from KD mice (Figures S8J–S8L), thus mirroring the alterations in MAM composition in Mfn2 L-KO mice. Overall, these results indicate that hepatic PSS1/2 deficiency recapitulates many of the hepatic alterations caused by Mfn2 ablation.

We next attempted to counter the liver alterations in L-KO mice by overexpressing PSS1 (Figure 4H). PSS1 overexpression led to an upregulation of Ptdss2 mRNA in L-KO mice (Figure 4I). As expected, we also found an increase in the synthesis of PS (Figure 4J), and surprisingly the normalization of liver triglycerides (Figure 4K). By contrast, PSS1 overexpression failed to rescue the synthesis of PE or PC (Figure 4J), or ameliorate the UPR (Figure 4L and S8M). Taken together, our data show that Mfn2 depletion causes a fundamental defect that prevents the synthesis of PE from PS.

Mfn2 is a PS-binding protein and generates PS-rich domains in membranes

A key process in the synthesis of phospholipids in MAMs is the transfer of PS and PE between the ER and mitochondria[20,22,25]. To determine whether Mfn2 was involved in PS transfer, we first investigated whether it binds phospholipids by assaying binding of

immunoprecipitated Mfn2 to lipid strips. Mfn2 was specifically immunoprecipitated under denaturing immunoprecipitation conditions with a polyclonal antibody. Mfn2 specifically bound phosphatidate (PA) and PS but not phosphatidylinositol (PI), PE or PC (Figure 5A). To validate this binding to phospholipids and to exclude the possibility that it was due to transmembrane domains, we constructed a truncated version of Mfn2 lacking the transmembrane domains and the C-terminal cytosolic portion (1–613), but preserving some metabolic characteristics of the full-length protein[62]. L-KO mice were tail vein injected with an adenoviral vector permitting the hepatic expression of this short form containing a 6×His tag at the N-terminus. We then purified the recombinant Mfn2 protein under denaturing conditions by affinity chromatography. Results showed that Mfn2 (1–613) could also specifically bind PS and PA (Figures 5B). To determine its potential *in vivo* role on phospholipid synthesis, we analyzed the effects on phospholipid synthesis by monitoring the incorporation of labeled L-Ser in the same L-KO mice. Data revealed that Mfn2 (1–613) enhanced the incorporation of L-Ser into PS, PE and PC (Figure 5C).

For *in vitro* analysis, we expressed Mfn2 (1–613) in *E. coli* and purified the protein by affinity chromatography that, after elution, represented >60% of the Comassie blue-stained proteins in gel electrophoresis (Figure 5D). Eluted Mfn2 (1–613) was also identified by mass spectrometry and contaminants were detected at very low levels (Supplementary Table 4). When we analyzed the capacity of the recombinant protein to bind phospholipids, we observed specific binding to PS and to PA in lipid strip assays (Figures 5E), consistent with the results in the liver. To exclude false positive binding due to phospholipid positioning in the strip, we performed liposome flotation assays, which confirmed that Mfn2 (1–613) mainly bound PS conjugated to a fluorophore (NBD) and also natural PS (Figures 5F and S9A) in liposomes. Overall, these data indicate that Mfn2 shows a capacity to selectively bind PS with minimal binding to natural PA and PI.

We next determined whether Mfn2 participates in the transfer of PS between membranes. We first evaluated its capacity to extract PS from liposomes, which may account for the alterations in the synthesis of PE in L-KO liver, even upon PSS1 overexpression. Phospholipid extraction was performed as described by Kawano et al[63]. Purified Mfn2 (1–613) was incubated with liposomes containing labeled phospholipids

(NBD-PS or NBD-PE) and the mixture was then separated by gradient centrifugation (Figure 5G). Subsequently, we analyzed the liposome-containing fraction and the non-liposome-containing fraction. Analysis of the distribution of NBD fluorescence in the presence of Mfn2 revealed that the fluorescence of NBD-PS decreased in the liposome fraction and increased in the non-liposome fraction (Figure 5H), whereas the distribution of NBD-PE fluorescence was unchanged both in the presence or absence of Mfn2 (Figure S9B).

In accord with these data, confocal microscopy revealed that Mfn2 (1–613) induced the formation of rigid domains containing exclusively NBD-PS (green color) from liposomes containing both NBD-PS (green) and Rhodamine-PE (red) (Figure 5I). Lipid domains were not generated when Mfn2 (1–613) was exposed to liposomes containing NBD-PC and Rhodamine-PE (Figure S9C). Given the unexpected capacity of Mfn2 (1–613) to generate PS-rich domains in membranes, we evaluated whether this capacity showed time-dependence and if it occurred with different types of liposomes. Using a well-established fluorescence resonance energy transfer-based membrane assay[64,65], we incubated control and Mfn2 (1–613) proteins with a mix of donor liposomes (containing NBD-phospholipids and Rhodamine-PE) and acceptor liposomes (non-fluorescent). The presence of Mfn2 (1–613) induced the release of NBD fluorescence in a time-dependent manner in liposomes containing NBD-PS but not NBD-PE (Figures 5J and S9D). Similar results were obtained using liposomes containing fluorescent TopFluor (TopFluor-PS or TopFluor-PE) derivatives of phospholipids, which are smaller in size than NBD-phospholipids (Figures S9E, and S9F). Our results support the view that Mfn2 binds PS and has the capacity to isolate it from membranes and to form rigid domains enriched in PS. These findings are consistent with a role for Mfn2 in exchanging lipids from different membranes or remodeling them in membranes, which may be due to lipid rearrangement.

PS-dependent remodeling activity of Mfn2 requires an intact N-terminal region

To address the specificity of Mfn2 functions, we tested whether Mfn1 has the same activities. To evaluate similar protein fragments in Mfn1 and in Mfn2, we expressed a recombinant truncated version of Mfn1 (1–592) in *E. coli*, which was purified under identical conditions as for Mfn2 (1–613) (Figure 6A). We first determined whether

Mfn1 (1–592) had phospholipid-binding activity. Liposome flotation assays revealed that, in contrast to Mfn2 (1–613), Mfn1 bound PC, PE, and PS phospholipids to a similar extent (Figure 6B). In a second analysis, lipid extraction assays revealed that Mfn1(1–592) failed to extract NBD-PS from liposomes (Figure 6C), but it did extract NBD-PE (Figure 6D), pointing to distinct functions for Mfn1 and Mfn2.

To better understand the basis for the differential capacity of Mfn1 and Mfn2 to bind and extract phospholipids, we examined the amino acid sequences of the two proteins (Figure 6E). Alignment analysis revealed that the N-terminal (20 aa residues) sequence of Mfn2 was absent in Mfn1. We then expressed and purified a mutant form of Mfn2 lacking this fragment (referred to as Mfn2 21–613) in *E.coli* (Figure 6F) and used it in liposome flotation assays. Results showed that Mfn2 (21–613) bound to PS, PE, PC (Figure 6G). Notably, lipid extraction assays revealed that purified Mfn2 (21–613) extracted both NBD-PS and NBD-PE from liposomes (Figure 6H and 6I). Thus, the Mfn2 (21–613) mutant combines the properties of both Mfn1 and Mfn2, suggesting that the N-terminal fragment is key to confer selectivity to extract PS.

Re-expression of Mfn2 in mice on MCD diet alleviates liver disease

After establishing the unique action of Mfn2 on phospholipid partition and metabolism, we next examined the consequences in liver under conditions of reduced Mfn2 expression during NASH. Specifically, we assessed whether the reduced Mfn2 levels in mice on MCD diet was linked to impaired PS transfer and whether it was key to the pathological alterations. We also investigated the possible role of ER stress in this scenario. Mice were placed on MCD or chow diet for two weeks and were then intravenously injected with a control adenovirus or with adenoviruses encoding Mfn2 or BIP, and livers were studied one week later. Hepatic Mfn2 expression was normalized in MCD mice upon injection of Mfn2 adenoviruses (Figures S10A, and S10C), whereas BIP failed to recover Mfn2 levels (Figures S10B and S10C). Compared with the control diet, the MCD diet induced an enhanced incorporation of radiolabeled L-Ser into PS, and a low synthesis of PE and PC in hepatic MAMs (Figure 7A). Mfn2 re-expression normalized the incorporation of L-Ser into PE and PC, whereas BIP did not ameliorate as Mfn2 the low levels of phospholipid synthesis (Figure 7A).

Analysis of fibrosis in liver sections of MCD diet-fed mice showed that Mfn2-re-expressing mice had less Sirius red staining than mice treated with control adenovirus (Figure 7B), whereas the expression of BIP only partially diminished fibrosis (Figure 7B). Similarly, triglyceride accumulation in liver was decreased upon Mfn2 re-expression as assessed by H&E staining (Figure 7B), and by quantification of triglycerides (Figure 7C). By contrast, BIP expression failed to normalize hepatic triglycerides in MCD diet-fed mice (Figure 7B, and 7C). As expected, the expression of inflammatory and fibrosis markers was markedly decreased by Mfn2 re-expression, but not by BIP overexpression (Figures 7D). Finally, both BIP and Mfn2 treatments normalized all UPR markers upregulated in MCD mice (Figure S10D).

Overall, our data strongly suggest that Mfn2 repression plays a key role in the development of steatosis, inflammation and fibrosis in a mouse model of NASH. Moreover, we have identified a defect in phospholipid synthesis in MCD diet-fed mice, which it is crucial for the development of the pathology. Our data are consistent with a major role of Mfn2 in the normalization of PS transfer from ER to mitochondria, which seems critical for the amelioration of liver disease.

Discussion

We report that Mfn2 plays a key role in liver homeostasis by controlling both PS transfer from ER to mitochondria and the UPR. Accordingly, hepatic ablation of Mfn2 results in unbalanced phospholipid metabolism, leading to ER stress and triggering liver inflammation and fibrosis, which takes place early in the life of these mice and occurs even on a normal diet and in the absence of obesity. In addition, mice with liver-specific knockout of Mfn2 have enhanced susceptibility to liver cancer with age or in response to carcinogenic agents. Supporting the clinical relevance of these findings, we show that hepatic Mfn2 expression is lower in patients with NASH than in those with steatosis. Mfn2 expression is also repressed in mouse models of steatosis and NASH, and its re-expression diminishes NASH-like liver pathologies. Taken together, our data indicate that hepatic Mfn2 is a key protein to maintain healthy liver function and its repression is involved in the development of liver disease.

We show that the UPR caused by Mfn2 deficiency plays a key role in the development of hepatic inflammation, apoptosis, compensatory proliferation and fibrosis, which in turn contributes to the development of liver cancer[48]. Thus, normalization of UPR response by BIP gain-of-function restores inflammation to control levels and reduces apoptosis, hyper-proliferation and fibrosis, which would prevent the development of cancer. These results are consistent with our previous observations that deficient hepatic insulin signaling is normalized in Mfn2 knockout mice treated with tauroursodeoxycholic acid[31]. Indeed, chronic ER stress plays a key role in the pathophysiology associated with Mfn2 deficiency, and appears to be responsible for the alterations in mitochondrial metabolism that have been detected in Mfn2-deficient cells[29]. The fact that inflammation, fibrosis and insulin resistance are modulated by ER stress may explain the relationship reported between steatosis, insulin resistance, and NASH[48,52,66-68].

We found that Mfn2 re-expression normalizes liver function in a mouse model of NASH, whereas BIP expression only partially counters steatosis, inflammation and fibrosis. These findings indicate that whereas Mfn2 likely plays a key role in the

development of liver disease in murine NASH, the UPR is a secondary contributing factor.

Our data also reveal that Mfn2 deficiency markedly impairs phospholipid metabolism and this lies upstream of the UPR. Thus, BIP-induced amelioration of UPR failed to normalize lipid metabolism. The changes in phospholipid metabolism associated with Mfn2 deficiency were characterized by lower rates of synthesis of PS, PE and PC, reduced expression of phosphatidylserine synthases PSS1 and PSS2, and reduced abundance of PSS1 in MAM fractions. We also found that a reduction in hepatic phospholipid metabolism explains the enhanced accumulation of triglycerides, the UPR and inflammation. While the re-expression of PSS1 was not sufficient to mitigate the defective synthesis of PE and PC in Mfn2-depleted livers, it significantly reduced hepatic triglycerides, revealing a close regulation of phospholipid and triglyceride synthesis in MAMs. Expression of both full-length and truncated Mfn2, lacking the transmembrane domains, improved phospholipid metabolism in Mfn2-deficient livers. Thus, our results indicate that loss of hepatic Mfn2 expression changes phospholipid metabolism by altering two different steps: 1) reducing the transfer of PS from the ER to mitochondria, and 2) inhibiting PS synthesis as a consequence of a compensatory reduced expression of PPS1 and PSS2.

Importantly, we describe a new molecular function of Mfn2 in the maintenance of hepatic phospholipid metabolism. Mfn2 has the capacity to bind PS *in vitro*, and to cause partitions of PS into rigid membrane domains. These activities are specific for PS and are not found with other phospholipids such as PE or PC. Indeed, these data may be key to understand the molecular basis for the multiple cellular effects of Mfn2[26,31,32,69]. In addition, our observations provide molecular insights into the steps involved in the transfer of PS from ER to mitochondria. We propose that Mfn2 participates in the generation of PS-enriched domains at the ER-mitochondria contact sites and they favor the activity of potential PS transport proteins such as the oxysterol-binding protein (OSBP)-related proteins ORPs (ORP5/ORP8) or VAT-1. ORP5/8 binds PS in vitro[70] and mediates PI4P/PS counter transport between the ER and the plasma membrane[71]. These proteins have also been identified in MAMs[72] and therefore may participate in the transfer of PS between ER and mitochondria.

The observation of a link between Mfn2 and phospholipids is highly relevant because of their influence on membrane-dependent cellular functions, antioxidant, anti-inflammatory, anti-fibrotic properties, and cellular signaling[73,74]. Thus, obesity has been reported to increase the hepatic PC/PE ratio which inhibits SERCA activity[75]. In addition, genetic inhibition of PEMT, which catalyzes the conversion of PE to PC, relieves ER stress and improves systemic glucose homeostasis in obesity[75,76]. Mfn2 levels are increased in MAMs in obese mice[56] under conditions in which enhanced PC production has been reported[75]. Furthermore, low levels of phospholipids in bile due to the disruption of membrane transporters are linked to liver disease[77,78]. Another important feature of our work is the observation that hepatic Mfn2 ablation provokes MAM remodeling similar to that detected in HFD or genetic obesity. This is also relevant because remodeling of MAM interactions in liver in obesity has been shown to result in undesirable side effects such as triacylglycerol accumulation and insulin resistance[56]. Specifically, hepatic MAM shows an enhanced abundance of protein markers such as PACS2, IP3R1, and IP3R2 during obesity[56], which is consistent with the pattern of changes detected in Mfn2-deficient livers. Accordingly, we propose that alterations in Mfn2 expression have an impact on MAM reorganization, perhaps through changes in the phospholipid composition in ER-mitochondrial contact sites. These observations also reveal that changes to Mfn2 levels may alter the composition of tethers at ER-mitochondrial contact sites, and this may be dependent on the cell context. In addition, those data complement the observations that disruption of individual MAM components seem to be sufficient to alter phospholipid synthesis in disorders such as Alzheimer disease and Lenz-Majewski syndrome[79-81].

In contrast to the function of Mfn2, Mfn1 shows a broader phospholipid binding activity but it does not generate PE- or PC-rich domains. The N-terminal region (20 amino acid residues) of Mfn2 (not present in Mfn1) is key for PS specificity, as elimination of this region generates a mutant form of Mfn2 incorporating the capacities of Mfn1 and Mfn2, indicating a hybrid behavior. Further studies will be needed to understand the molecular basis for the PS binding and extraction activities of Mfn2.

In conclusion, our data support the view that Mfn2 sustains PS transfer to the mitochondria for conversion to PE. The effects on phospholipid metabolism may explain the role of Mfn2 in the maintenance of MAMs and proper lipid metabolism and

ER homeostasis. Thus, we propose Mfn2 as a potential therapeutic target for counteracting the development of liver disease related to NASH and liver cancer.

Experimental Procedures.

Experimental Procedures see Supplemental Information.

Author contributions

M.I.H.-A. conceived, designed the study and the strategy, performed experiments, discussed the results and wrote the manuscript; D. Sebastián, S.V., P.B., P.K., N.P., S.R.V., V.H., N.V., P.G., A.A., M.J.,R.P., I.G., E.C.,N.C., R.C., A.K., M.B., D.S., T.H., J.F., E.E-M, M.O., J.J., performed experiments; S.I. conceived and performed experiments; A.B-L performed the total liver lipidomics statistical analysis; M.O, C.C. M.P., S.F-V and J.V. revised experimental data and contributed to the discussion. A.Z. designed the study and the strategy, discussed the results, and wrote the manuscript.

Acknowledgements.

We thank Dr. Jennifer Rieusset for the BIP adenovirus and Dr. Estela Area-Gomez for sharing with us the protocol of phospholipid synthesis. We also thank the Unit of Electron Cryo-Microscopy (Scientific and Technological Centers, *Universitat de Barcelona*), Dr. Mar García-Rocha for discussion and Jorge Manuel Seco for technological assistance. We thank Dr. Helena Cortez-Pinto (Department of Gastroenterology, Hospital Santa Maria, Lisbon, Portugal) for providing the liver biopsies. We thank Neus Prats and the histopathology facility for the pathologic analysis of the mouse samples. We thank also the protein expression core facility for the production of short form Mfn2 in *E. coli*. M.I. Hernández-Alvarez was the recipient of a predoctoral fellowship from the CONACYT, Mexico, and is recipient of a postdoctoral fellowship "Juan de la Cierva Incorporación". This study was supported by research grants from the MINECO (SAF2016-75246R), Grant 2014SGR48 from the *Generalitat de Catalunya*, INFLAMES (PIE-14/00045) from the Instituto de Salud Carlos III, CIBERDEM ("Instituto de Salud Carlos III"), and INTERREG IV-B-SUDOE-FEDER (DIOMED, SOE1/P1/E178). A.Z. is a recipient of an ICREA "Academia" (*Generalitat*

de Catalunya). We gratefully acknowledge institutional funding from the MINECO through the Centres of Excellence Severo Ochoa Award, and from the CERCA Program of the Generalitat de Catalunya.

References.

1. Chalasani, N.*, et al.* The diagnosis and management of non-alcoholic fatty liver disease: practice Guideline by the American Association for the Study of Liver Diseases, American College of Gastroenterology, and the American Gastroenterological Association. *Hepatology* **55**, 2005-2023 (2012).
2. Yeh, M.M. & Brunt, E.M. Pathological features of fatty liver disease. *Gastroenterology* **147**, 754-764 (2014).
3. Brenner, C., Galluzzi, L., Kepp, O. & Kroemer, G. Decoding cell death signals in liver inflammation. *Journal of Hepatology* **59**, 583-594 (2013).
4. Aravalli, R.N., Steer, C.J. & Cressman, E.N. Molecular mechanisms of hepatocellular carcinoma. *Hepatology* **48**, 2047-2063 (2008).
5. Aravalli, R.N., Cressman, E.N. & Steer, C.J. Cellular and molecular mechanisms of hepatocellular carcinoma: an update. *Arch Toxicol* **87**, 227-247 (2013).
6. Demaria, S.*, et al.* Cancer and inflammation: promise for biologic therapy. *J Immunother* **33**, 335-351 (2010).
7. Mantovani, A., Allavena, P., Sica, A. & Balkwill, F. Cancer-related inflammation. *Nature* **454**, 436-444 (2008).
8. Grivennikov, S.I., Greten, F.R. & Karin, M. Immunity, inflammation, and cancer. *Cell* **140**, 883-899 (2010).
9. Coussens, L.M. & Werb, Z. Inflammation and cancer. *Nature* **420**, 860-867 (2002).
10. Tilg, H. & Hotamisligil, G.S. Nonalcoholic fatty liver disease: Cytokine-adipokine interplay and regulation of insulin resistance. *Gastroenterology* **131**, 934-945 (2006).
11. Dumas, M.E.*, et al.* Metabolic profiling reveals a contribution of gut microbiota to fatty liver phenotype in insulin-resistant mice. *Proceedings of the National Academy of Sciences of the United States of America* **103**, 12511-12516 (2006).
12. Miele, L.*, et al.* Increased intestinal permeability and tight junction alterations in nonalcoholic fatty liver disease. *Hepatology* **49**, 1877-1887 (2009).
13. Dara, L., Ji, C. & Kaplowitz, N. The contribution of endoplasmic reticulum stress to liver diseases. *Hepatology* **53**, 1752-1763 (2011).
14. Alkhouri, N., Dixon, L.J. & Feldstein, A.E. Lipotoxicity in nonalcoholic fatty liver disease: not all lipids are created equal. *Expert review of gastroenterology & hepatology* **3**, 445-451 (2009).
15. Begriche, K., Massart, J., Robin, M.A., Bonnet, F. & Fromenty, B. Mitochondrial adaptations and dysfunctions in nonalcoholic fatty liver disease. *Hepatology* **58**, 1497-1507 (2013).
16. Schenkel, L.C. & Bakovic, M. Formation and Regulation of Mitochondrial Membranes. *International Journal of Cell Biology* **2014**, 13 (2014).
17. Tatsuta, T., Scharwey, M. & Langer, T. Mitochondrial lipid trafficking. *Trends in Cell Biology* **24**, 44-52 (2014).
18. Ardail, D.*, et al.* Mitochondrial contact sites. Lipid composition and dynamics. *Journal of Biological Chemistry* **265**, 18797-18802 (1990).
19. Paradies, G., Paradies, V., Ruggiero, F.M. & Petrosillo, G. Oxidative stress, cardiolipin and mitochondrial dysfunction in nonalcoholic fatty liver disease. *World Journal of Gastroenterology : WJG* **20**, 14205-14218 (2014).
20. Osman, C., Voelker, D.R. & Langer, T. Making heads or tails of phospholipids in mitochondria. *The Journal of Cell Biology* **192**, 7-16 (2011).
21. Flis, V.V. & Daum, G. Lipid Transport between the Endoplasmic Reticulum and Mitochondria. *Cold Spring Harbor Perspectives in Biology* **5**(2013).
22. Raturi, A. & Simmen, T. Where the endoplasmic reticulum and the mitochondrion tie the knot: The mitochondria-associated membrane (MAM). *Biochimica et Biophysica Acta (BBA) - Molecular Cell Research* **1833**, 213-224 (2013).

23. Vance, J.E. & Vance, D.E. Phospholipid biosynthesis in mammalian cells. *Biochemistry and Cell Biology* **82**, 113-128 (2004).
24. Scharwey, M., Tatsuta, T. & Langer, T. Mitochondrial lipid transport at a glance. *Journal of Cell Science* **126**, 5317-5323 (2013).
25. Shiao, Y.J., Balcerzak, B. & Vance, J.E. A mitochondrial membrane protein is required for translocation of phosphatidylserine from mitochondria-associated membranes to mitochondria. *Biochemical Journal* **331**, 217-223 (1998).
26. de Brito, O.M. & Scorrano, L. Mitofusin 2 tethers endoplasmic reticulum to mitochondria. *Nature* **456**, 605-610 (2008).
27. Leal, N.S*., et al.* Mitofusin-2 knockdown increases ER-mitochondria contact and decreases amyloid beta-peptide production. *J Cell Mol Med* **20**, 12863 (2016).
28. Wang, L*., et al.* Mitofusin 2 Regulates Axonal Transport of Calpastatin to Prevent Neuromuscular Synaptic Elimination in Skeletal Muscles. *Cell metabolism* **28**, 400-414 e408 (2018).
29. Muñoz, J.P*., et al.* Mfn2 modulates the UPR and mitochondrial function via repression of PERK. *The EMBO journal* **32**, 2348-2361 (2013).
30. Schneeberger, M*., et al.* Mitofusin 2 in POMC neurons connects ER stress with leptin resistance and energy imbalance. *Cell* **155**, 172-187 (2013).
31. Sebastián, D*., et al.* Mitofusin 2 (Mfn2) links mitochondrial and endoplasmic reticulum function with insulin signaling and is essential for normal glucose homeostasis. *Proceedings of the National Academy of Sciences* **109**, 5523-5528 (2012).
32. Bach, D*., et al.* Mitofusin-2 Determines Mitochondrial Network Architecture and Mitochondrial Metabolism: A NOVEL REGULATORY MECHANISM ALTERED IN OBESITY. *Journal of Biological Chemistry* **278**, 17190-17197 (2003).
33. Pich, S*., et al.* The Charcot–Marie–Tooth type 2A gene product, Mfn2, up-regulates fuel oxidation through expression of OXPHOS system. *Human Molecular Genetics* **14**, 1405-1415 (2005).
34. Rehman, J*., et al.* Inhibition of mitochondrial fission prevents cell cycle progression in lung cancer. *Faseb J* **26**, 2175-2186 (2012).
35. Wang, W*., et al.* Pro-apoptotic and anti-proliferative effects of mitofusin-2 via Bax signaling in hepatocellular carcinoma cells. *Med Oncol* **29**, 70-76 (2012).
36. Xu, K*., et al.* MFN2 suppresses cancer progression through inhibition of mTORC2/Akt signaling. *Sci Rep* **7**(2017).
37. Cheng, X., Zhou, D., Wei, J. & Lin, J. Cell-cycle arrest at G2/M and proliferation inhibition by adenovirus-expressed mitofusin-2 gene in human colorectal cancer cell lines. *Neoplasma* **60**, 620-626 (2013).
38. Wu, Y*., et al.* Clinical significance of mitofusin-2 and its signaling pathways in hepatocellular carcinoma. *World J Surg Oncol* **14**, 016-0922 (2016).
39. Zhou, X*., et al.* MicroRNA-761 is upregulated in hepatocellular carcinoma and regulates tumorigenesis by targeting Mitofusin-2. *Cancer Sci* **107**, 424-432 (2016).
40. Qu, L., Chen, H., Wang, G. & Wei, J. Frequent losses of heterozygosity in the mitofusin 2 gene in hepatocellular carcinoma: their relationship to clinicopathological features. *Tumori* **99**, 697-701 (2013).
41. Ferreira, D.M.S*., et al.* Apoptosis and insulin resistance in liver and peripheral tissues of morbidly obese patients is associated with different stages of non-alcoholic fatty liver disease. *Diabetologia* **54**, 1788-1798 (2011).
42. Takeda, D*., et al.* Effect of preoperative chemotherapy on postoperative liver regeneration following hepatic resection as estimated by liver volume. *World J Surg Oncol* **11**, 1477-7819 (2013).
43. Gaemers, I.C*., et al.* Lipotoxicity and steatohepatitis in an overfed mouse model for non-alcoholic fatty liver disease. *Biochimica et Biophysica Acta (BBA) - Molecular Basis of Disease* **1812**, 447-458 (2011).

44. Matsumoto, M.*, et al.* An improved mouse model that rapidly develops fibrosis in non-alcoholic steatohepatitis. *International Journal of Experimental Pathology* **94**, 93-103 (2013).
45. Malhi, H., Guicciardi, M.E. & Gores, G.J. Hepatocyte death: a clear and present danger. *Physiological reviews* **90**, 1165-1194 (2010).
46. Sun, B. & Karin, M. Obesity, inflammation, and liver cancer. *J Hepatol* **56**, 704-713 (2012).
47. Herranz, D.*, et al.* Sirt1 improves healthy ageing and protects from metabolic syndrome-associated cancer. *Nat Commun* **1**, 3 (2010).
48. DeZwaan-McCabe, D.*, et al.* The Stress-Regulated Transcription Factor CHOP Promotes Hepatic Inflammatory Gene Expression, Fibrosis, and Oncogenesis. *PLoS Genet* **9**, e1003937 (2013).
49. Sch, #xf6 & nthal, A.H. Endoplasmic Reticulum Stress: Its Role in Disease and Novel Prospects for Therapy. *Scientifica* **2012**, 26 (2012).
50. Lee, A.S. The glucose-regulated proteins: stress induction and clinical applications. *Trends in Biochemical Sciences* **26**, 504-510 (2001).
51. Fagone, P. & Jackowski, S. Membrane phospholipid synthesis and endoplasmic reticulum function. *Journal of Lipid Research* **50**, S311-S316 (2009).
52. Fu, S.*, et al.* Aberrant lipid metabolism disrupts calcium homeostasis causing liver endoplasmic reticulum stress in obesity. *Nature* **473**, 528-531 (2011).
53. Halbleib, K.*, et al.* Activation of the Unfolded Protein Response by Lipid Bilayer Stress. *Molecular Cell* **67**, 673-684.e678.
54. Singaravelu, K.*, et al.* Mitofusin 2 regulates STIM1 migration from the Ca2+ store to the plasma membrane in cells with depolarized mitochondria. *The Journal of biological chemistry* **286**, 12189-12201 (2011).
55. Stone, S.J. & Vance, J.E. Phosphatidylserine Synthase-1 and -2 Are Localized to Mitochondria-associated Membranes. *Journal of Biological Chemistry* **275**, 34534-34540 (2000).
56. Arruda, A.P.*, et al.* Chronic enrichment of hepatic endoplasmic reticulum-mitochondria contact leads to mitochondrial dysfunction in obesity. *Nat Med* **20**, 1427-1435 (2014).
57. Steenbergen, R., Nanowski, T.S., Nelson, R., Young, S.G. & Vance, J.E. Phospholipid homeostasis in phosphatidylserine synthase-2-deficient mice. *Biochimica et Biophysica Acta (BBA) - Molecular and Cell Biology of Lipids* **1761**, 313-323 (2006).
58. STONE, S.J. & VANCE, J.E. Cloning and expression of murine liver phosphatidylserine synthase (PSS)-2: differential regulation of phospholipid metabolism by PSS1 and PSS2. *Biochemical Journal* **342**, 57-64 (1999).
59. Vance, J.E. & Tasseva, G. Formation and function of phosphatidylserine and phosphatidylethanolamine in mammalian cells. *Biochimica et Biophysica Acta (BBA) - Molecular and Cell Biology of Lipids* **1831**, 543-554 (2013).
60. Bergo, M.O.*, et al.* Defining the Importance of Phosphatidylserine Synthase 2 in Mice. *Journal of Biological Chemistry* **277**, 47701-47708 (2002).
61. Arikketh, D., Nelson, R. & Vance, J.E. Defining the Importance of Phosphatidylserine Synthase-1 (PSS1): Unexpected Viability of PSS1-Deficient Mice. *Journal of Biological Chemistry* **283**, 12888-12897 (2008).
62. Segales, J.*, et al.* A form of mitofusin 2 (Mfn2) lacking the transmembrane domains and the COOH-terminal end stimulates metabolism in muscle and liver cells. *Am J Physiol Endocrinol Metab* **305**, 13 (2013).
63. Kawano, S.*, et al.* Structure-function insights into direct lipid transfer between membranes by Mmm1-Mdm12 of ERMES. *J Cell Biol* **217**, 959-974 (2018).
64. Connerth, M.*, et al.* Intramitochondrial Transport of Phosphatidic Acid in Yeast by a Lipid Transfer Protein. *Science* **338**, 815-818 (2012).

65. Potting, C*., et al.* TRIAP1/PRELI complexes prevent apoptosis by mediating intramitochondrial transport of phosphatidic acid. *Cell metabolism* **18**, 287-295 (2013).
66. Longato, L*., et al.* Insulin Resistance, Ceramide Accumulation, and Endoplasmic Reticulum Stress in Human Chronic Alcohol-Related Liver Disease. *Oxidative Medicine and Cellular Longevity* **2012**, 17 (2012).
67. Tilg, H. & Moschen, A.R. Evolution of inflammation in nonalcoholic fatty liver disease: The multiple parallel hits hypothesis. *Hepatology* **52**, 1836-1846 (2010).
68. Pagliassotti, M.J. Endoplasmic Reticulum Stress in Nonalcoholic Fatty Liver Disease. *Annual Review of Nutrition* **32**, 17-33 (2012).
69. Koshiba, T*., et al.* Structural basis of mitochondrial tethering by mitofusin complexes. *Science* **305**, 858-862 (2004).
70. Maeda, K*., et al.* Interactome map uncovers phosphatidylserine transport by oxysterol-binding proteins. *Nature* **501**, 257-261 (2013).
71. Chung, J*., et al.* INTRACELLULAR TRANSPORT. PI4P/phosphatidylserine countertransport at ORP5- and ORP8-mediated ER-plasma membrane contacts. *Science* **349**, 428-432 (2015).
72. Galmes, R*., et al.* ORP5/ORP8 localize to endoplasmic reticulum-mitochondria contacts and are involved in mitochondrial function. *EMBO Rep* **17**, 800-810 (2016).
73. Gundermann, K.J., Kuenker, A., Kuntz, E. & Drozdzik, M. Activity of essential phospholipids (EPL) from soybean in liver diseases. *Pharmacol Rep* **63**, 643-659 (2011).
74. Chakravarthy, M.V*., et al.* Identification of a physiologically relevant endogenous ligand for PPARalpha in liver. *Cell* **138**, 476-488 (2009).
75. Fu, S*., et al.* Aberrant lipid metabolism disrupts calcium homeostasis causing liver endoplasmic reticulum stress in obesity. *Nature* **473**, 528-531 (2011).
76. Jacobs, R.L*., et al.* Impaired de novo choline synthesis explains why phosphatidylethanolamine N-methyltransferase-deficient mice are protected from diet-induced obesity. *The Journal of biological chemistry* **285**, 22403-22413 (2010).
77. Tanaka, N., Matsubara, T., Krausz, K.W., Patterson, A.D. & Gonzalez, F.J. Disruption of phospholipid and bile acid homeostasis in mice with nonalcoholic steatohepatitis. *Hepatology* **56**, 118-129 (2012).
78. Tarling, E.J., de Aguiar Vallim, T.Q. & Edwards, P.A. Role of ABC transporters in lipid transport and human disease. *Trends in endocrinology and metabolism: TEM* **24**, 342-350 (2013).
79. Area-Gomez, E*., et al. Upregulated function of mitochondria-associated ER membranes in Alzheimer disease*, (2012).
80. Area-Gomez, E. & Schon, E.A. Mitochondrial Genetics and Disease. *Journal of Child Neurology* **29**, 1208-1215 (2014).
81. Sousa, S.B*., et al.* Gain-of-function mutations in the phosphatidylserine synthase 1 (PTDSS1) gene cause Lenz-Majewski syndrome. *Nat Genet* **46**, 70-76 (2014).

FIGURE LEGENDS.

FIGURE 1. Mfn2 is reduced in NASH and liver-specific Mfn2 ablation in mice causes a NASH-like phenotype. A) Quantification of Mfn2 protein in liver biopsies from steatotic (NAS ≤3, n=7) and NASH (NAS ≥5, n=8) patients. B) Quantification of Mfn2 protein in liver from mice on chow diet (C) or high-fat diet (HFD) as a model of steatosis (n=4 mice per group). C) Representative H&E and Sirius red staining images in liver sections from 8-week-old C57Bl6/J mice fed either a chow diet (C) or a methionine/choline-deficient diet combined with HFD and supplemented with 0.1% L-methionine in drinking water (MCD) (scale bar, 200 μm). D) Triglyceride (TAG) levels in liver from mice on C and MCD diets (n=5 mice per group). E) Quantification of Mfn2 protein in liver from C (n=5) and MCD mice (n=4). F) Hepatic pro-inflammatory factors in control (C) and liver-specific Mfn2 KO (L-KO) mice measured by ELISA (n=8 mice per group). G) Hepatic TAG levels in C and L-KO mice (n=8–12 mice per group). H) Oleate incorporation into different lipid species in hepatocytes isolated from C and L-KO mice (n=4 mice per group, each experiment performed in triplicate). I) Representative Sirius red staining and TEM images in liver sections from 27-week-old C and L-KO mice fed a normal diet (scale bars, 200 μm in Sirius Red staining images, and 5 μm in TEM images). J) Hepatic expression of genes involved in collagen synthesis in C and L-KO mice (n=5 mice per group). K) Representative macroscopic images of liver from 24 month-old C and L-KO mice fed a normal diet, and quantification of liver tumors expressed as the mean of number of tumours in livers from 5 mice. In panel A, data are expressed as mean ± SD, and in the remaining panels as mean ± SE. *$p<0.05$ vs. control group in each case.

FIGURE 2. Normalization of ER stress ameliorates inflammation and fibrosis but not lipid metabolism in L-KO mice. Control (C) mice were studied 5 days after tail vein injection of control LacZ adenoviruses (C+AdC) and L-KO mice were studied 5 days after tail vein injection of control (LacZ) (L-KO+AdC, red bars) or BIP adenoviruses (L-KO+AdBIP, yellow bars) (n=4 mice per group). Data are expressed as values relative to control LacZ group (shown as a discontinuous line). A) Representative western blot of protein expression of hepatic ER stress markers. B)

Hepatic pro-inflammatory factors measured by ELISA. C) Plasma levels of IL-1β. D) Expression of genes involved in collagen synthesis. E) Hepatic TAG levels . F) Oleate incorporation into lipid species in isolated hepatocytes. Data are expressed as mean ± SE. Statistical analysis was performed by using one-way ANOVA followed by post-hoc t tests. *$p<0.05$ L-KO vs. C mice, $^{\$}p<0.05$ L-KO+AdBIP vs. L-KO+AdC mice.

FIGURE 3. Mfn2 ablation alters hepatic phospholipid metabolism independently of ER stress. A) Hepatic phosphatidylcholine (PC) and phosphatidylethanolamine (PE) content measured by lipidomics in control (C) (n=11) and L-KO (n=13) mice. Data are expressed as fold-change vs. C mice. Significant compounds are shown in the heatmap ($p<0.05$) out of 128 phospholipids analyzed. B) Graphical scheme of phosphatidylserine (PS), phosphatidylethanolamine (PE) and PS synthesis in mitochondria-associated ER membranes (MAMs). C–E) ^{3}H- L-serine incorporation into PS (C), PE (D), and phosphatidylcholine (PC) (E) in hepatic mitochondria-associated ER-enriched fractions from C and L-KO mice (n=5–7 mice per group). F) ^{3}H- L-serine incorporation into PS, PE and PC in hepatic mitochondria-associated ER-enriched fractions from control (lacZ injected, C+AdC), L-KO (lacZ injected, L-KO+AdC, red bars), and L-KO (BIP injected, L-KO+BIP mice, yellow bars) (n=4 mice per group). Data are expressed as values relative to C+AdC group (shown as a discontinuous line). G) ^{3}H-L-serine incorporation into PS, PE and PC in hepatic mitochondria-associated ER-enriched fractions from C+AdC, L-KO+AdC (red bars), and L-KO (Mfn2 injected, L-KO+AdMfn2 mice, grey bars) (n=4 mice per group). Data are expressed as values relative to C+AdC group (shown as a discontinuous line). H) Representative western blot showing hepatic expression of PSS1, PSS2 and PEMT proteins levels in 8-week-old C and L-KO mice (n=4 mice per group). I) Protein expression of MAM proteins in liver from C and L-KO mice (n=4 mice per group). Data are expressed as mean ± SE. Statistical analysis was performed by using one-way ANOVA followed by post-hoc t tests. *$p<0.05$ L–KO vs. C mice, $^{\$}p<0.05$ vs. L-KO+AdC mice.

FIGURE 4. Deficiency of hepatic phosphatidylserine synthase 1 and 2 phenocopies Mfn2 ablation. A) Quantification of hepatic protein expression of PSS1 and PSS2 5 days after tail vein injection with control LacZ (C) or Ptdss1/Ptdss2 (KD) siRNA

adenoviruses (n=5 mice per group). B) Quantification of PSS1 protein in MAM fractions obtained from C or KD mice (n=5 mice per group). C) ^{3}H-L-serine incorporation into PS and PE in hepatic mitochondria-associated ER-enriched fractions from C or KD mice (n=4 mice per group). D) Hepatic triglyceride (TAG) levels in C and KD mice (n=4 mice per group). E) Quantification of protein expression of hepatic ER stress markers in C and KD mice (n=4 mice per group). F) Hepatic expression of genes involved in inflammation in C and KD mice (n=5 mice per group). G) Quantification of Mfn2 protein in MAM fractions from C and KD mice. H) Scheme of PSS1 overexpression in mice. I) mRNA levels of Ptdss1 and Ptdss2 from control (lacZ injected, C+AdC), L-KO (lacZ injected, L-KO+AdC, red bars), and L-KO (Ptdss1 injected, L-KO+Ptdss1, blue bars) mice (n=3–5 mice per group). J) ^{3}H-L-serine incorporation into PS, PE and PC in hepatic mitochondria-associated ER-enriched fractions from C+AdC, L-KO+AdC (red bars), and L-KO+Ptdss1 mice (blue bars) (n=3–5 mice per group). K) Hepatic TAG levels in C+AdC, L-KO+AdC (red bars), and L-KO+Ptdss1 (blue bars) mice. L) Quantification of protein expression of hepatic ER stress markers in C+AdC, L-KO+AdC (red bars), and L-KO+Ptdss1 (blue bars) mice (n=3–5 mice per group). Data are expressed as values relative to C+AdC group (shown as a discontinuous line). Data are expressed as mean ± SE. Statistical analysis was performed by using one-way ANOVA followed by post-hoc t tests. *$p<0.05$ vs. C mice, $^{\$}p<0.05$ vs. L-KO+AdC mice.

FIGURE 5. Mfn2 binds phosphatidylserine and generates phosphatidylserine-rich domains in membranes. A) Binding of Mfn2 protein immunoprecipitated from liver to different phospholipids on a Membrane Lipid Strip^{TM}. B) Binding of a truncated form of Mfn2 (1–613), expressed in liver and purified by affinity chromatography, to phospholipids on a Membrane Lipid Strip^{TM}. C) ^{3}H-L-serine incorporation into PS, PE and PC in hepatic mitochondria-associated ER-enriched fractions from mice injected with LacZ in control (C+AdC) and L-KO (L-KO+AdC, red bars) mice and with a Mfn2 (1–613) adenovirus (L-KO+Mfn2 (1–613), blue bars) (n=4 mice per group). Data are expressed as values relative to the C+AdC group (shown as a discontinuous line). D) Representative Commassie-stained gel of the purification of Mfn2 (1–613) expressed in *E. coli*. E) Binding of Mfn2 (1–613) expressed in *E. coli* to different phospholipids on a Membrane Lipid Strip^{TM}. F) Representative western blot against Mfn2 after the

liposome flotation assay with different fluorescent (NBD) phospholipids. G) Scheme of the NBD-Phospholipid liposome extraction assay. H) Quantification of NBD-PS liposome extraction assay with Mfn2 (1–613) expressed in *E. coli* (n=6). I) Confocal microscopy images of liposomes in the absence or presence of Mfn2 (1–613), showing the formation of the NBD-PS rigid domain with Mfn2 (1–613). J) Kinetic FRET assay with NBD-PS and Rhod-PE to evaluate the capacity of Mfn2 (1–613) to dequench NBD-PS fluorescence from liposomes (n=6). Data are expressed as mean ± SE. Statistical analysis in panel H: *p<0.05 vs. C $p<0.05 vs. L-KO+AdC. Statistical analysis in panel J was performed by using a two-way ANOVA (*p<0.0001).

FIGURE 6. Phosphatidylserine binding and extraction activities of Mfn2 require an intact N-terminal region. A) Representative Commassie-stained gel of the purification of a short form of Mfn1 (1–592) expressed in *E. coli*. B) Representative western blot against histidine showing Mfn1 protein after the liposome flotation assay with different non-fluorescent phospholipids. C) Quantification of NBD-PS liposome extraction assay with Mfn1 (1–592) expressed in *E. coli* (n=3). D) Quantification of NBD-PE extraction assay with Mfn1 (1–592) expressed in *E. coli* (n=3). E) Mfn2 and Mfn1 human sequence alignment. F) Representative Commassie-stained gel of purification of Mfn2 (21–613) expressed in *E. coli*. G) Representative western blot against histidine showing Mfn2 (21–613) protein after the liposome flotation assay with non-fluorescent phospholipids. H) Quantification of NBD-PS liposome extraction assay with Mfn2 (21–613) expressed in *E. coli* (n=3). I) Quantification of NBD-PE liposome extraction assay with Mfn2 (21–613) expressed in *E. coli* (n=3). Data are expressed as mean ± SE. *p<0.05 vs. C.

FIGURE 7. Mfn2 re-expression improves the NASH phenotype in mice. A) ^{3}H-L-serine incorporation into PS, PE and PC in hepatic mitochondria-associated ER-enriched fractions from control mice injected with AdC (null adenovirus) (C+AdC, white bars), MCD mice injected with AdC (MCD+AdC, blue bars), with AdMfn2 (MCD+AdMfn2, red bars) or with AdBIP (MCD+BIP, yellow bars) (n=4 mice per group). B) Representative H&E and Sirius red staining images in liver sections from C+AdC, MCD+AdC, MCD+Mfn2 and MCD+BIP mice (scale bar, 200 μm). C) Hepatic

triglyceride (TAG) levels in C+AdC (white bars), MCD+AdC (blue bars), MCD+Mfn2 (red bars) and MCD+BIP (yellow bars) mice (n=4 mice per group). D) Hepatic pro-inflammatory factors and genes involved in collagen synthesis in C+AdC (white bars), MCD+AdC (blue bars), MCD+Mfn2 (red bars) and MCD+BIP (yellow bars) mice (n=4 mice per group). Data are expressed as the mean ± SE. Statistical analysis was performed by using one-way ANOVA followed by post-hoc t tests. *$p<0.05$ vs. C+AdC, $^{\$}p<0.05$ vs. MCD+AdC and $^{\#}p<0.05$ vs. MCD+AdBIP.

Figure 1

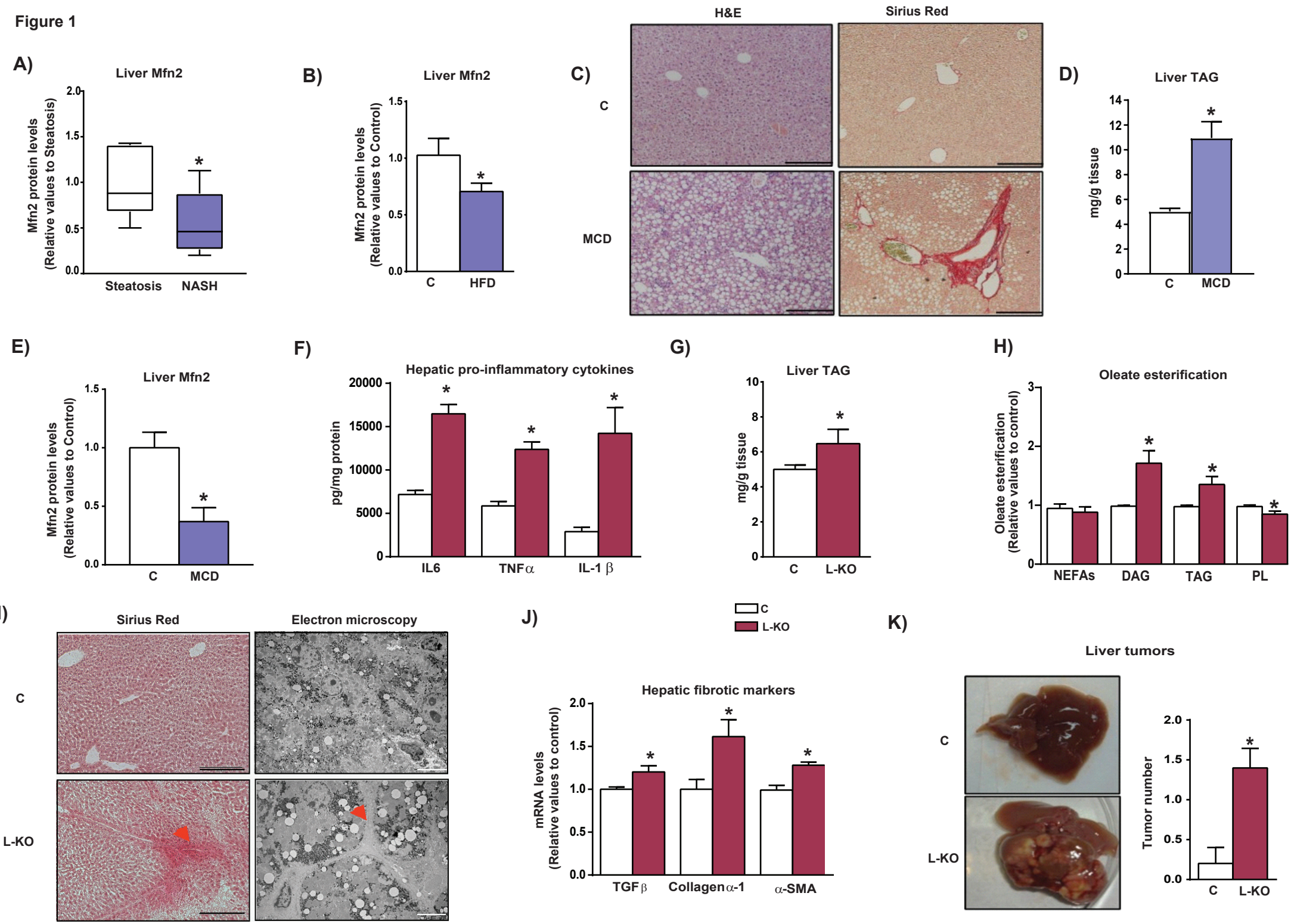
A)
Liver Mfn2
Mfn2 protein levels (Relative values to Steatosis)
2.0
1.5
1.0
0.5
0.0
*
Steatosis
NASH
B)
Liver Mfn2
Mfn2 protein levels (Relative values to Control)
1.5
1.0
0.5
0.0
*
C
HFD
C)
H&E
Sirius Red
C
MCD
D)
Liver TAG
mg/g tissue
14
12
10
8
6
4
2
0
*
C
MCD
E)
Liver Mfn2
Mfn2 protein levels (Relative values to Control)
1.5
1.0
0.5
0.0
*
C
MCD
F)
Hepatic pro-inflammatory cytokines
pg/mg protein
20000
15000
10000
5000
0
*
*
*
IL6
TNFα
IL-1 β
G)
Liver TAG
mg/g tissue
10
8
6
4
2
0
*
C
L-KO
H)
Oleate esterification
Oleate esterification (Relative values to control)
3
2
1
0
*
*
*
NEFAs
DAG
TAG
PL
I)
Sirius Red
Electron microscopy
C
L-KO
J)
C
L-KO
Hepatic fibrotic markers
mRNA levels (Relative values to control)
2.0
1.5
1.0
0.5
0.0
*
*
*
TGF β
Collagen α-1
α-SMA
K)
Liver tumors
C
L-KO
Tumor number
2.0
1.5
1.0
0.5
0.0
*
C
L-KO

Figure 2

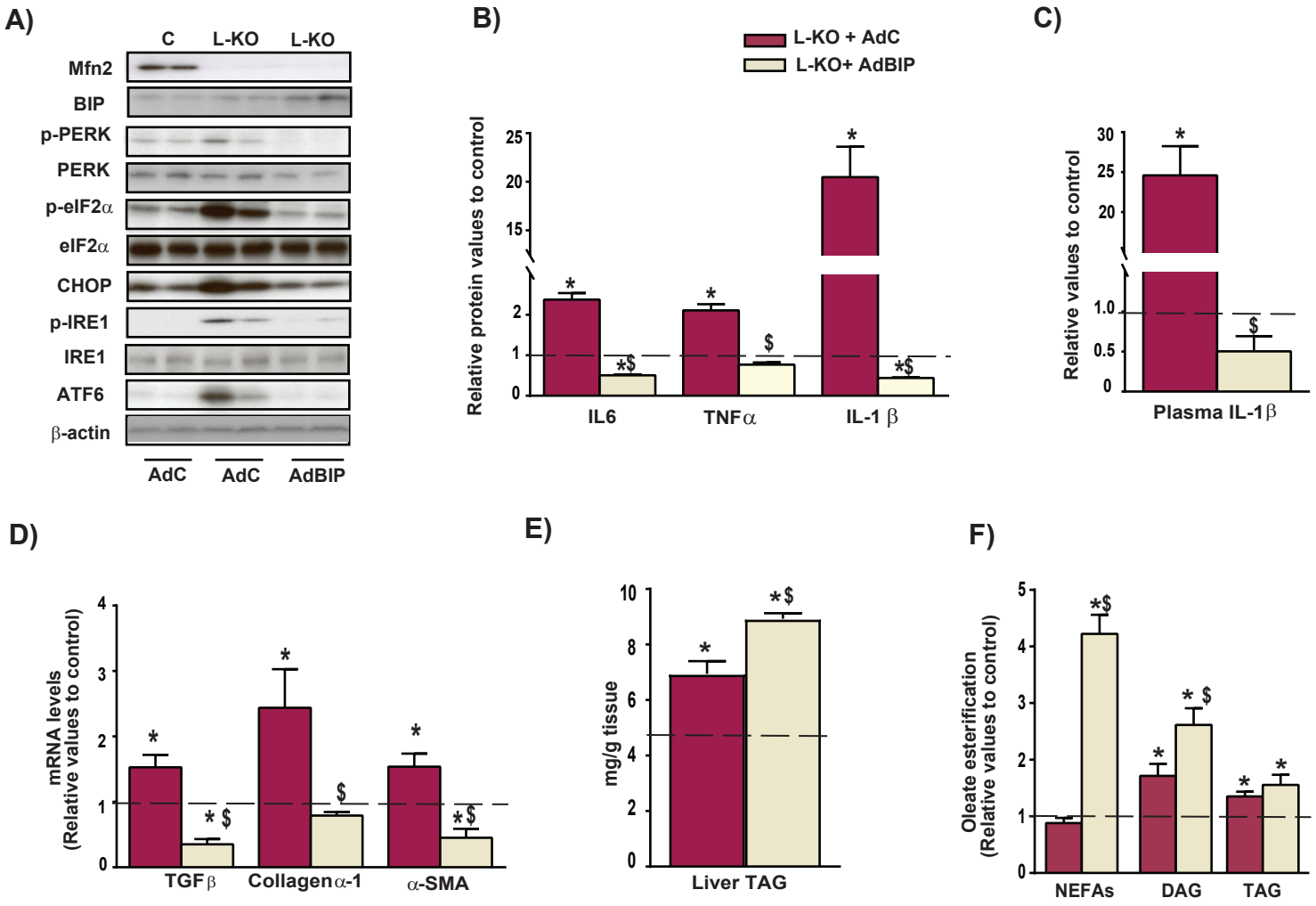
A)
C
L-KO
L-KO
Mfn2
BIP
p-PERK
PERK
p-eIF2α
eIF2α
CHOP
p-IRE1
IRE1
ATF6
β-actin
AdC
AdC
AdBIP
B)
L-KO + AdC
L-KO+ AdBIP
Relative protein values to control
IL6
TNFα
IL-1 β
C)
Relative values to control
Plasma IL-1β
D)
mRNA levels
(Relative values to control)
TGFβ
Collagen α-1
α-SMA
E)
mg/g tissue
Liver TAG
F)
Oleate esterification
(Relative values to control)
NEFAs
DAG
TAG

Figure 3

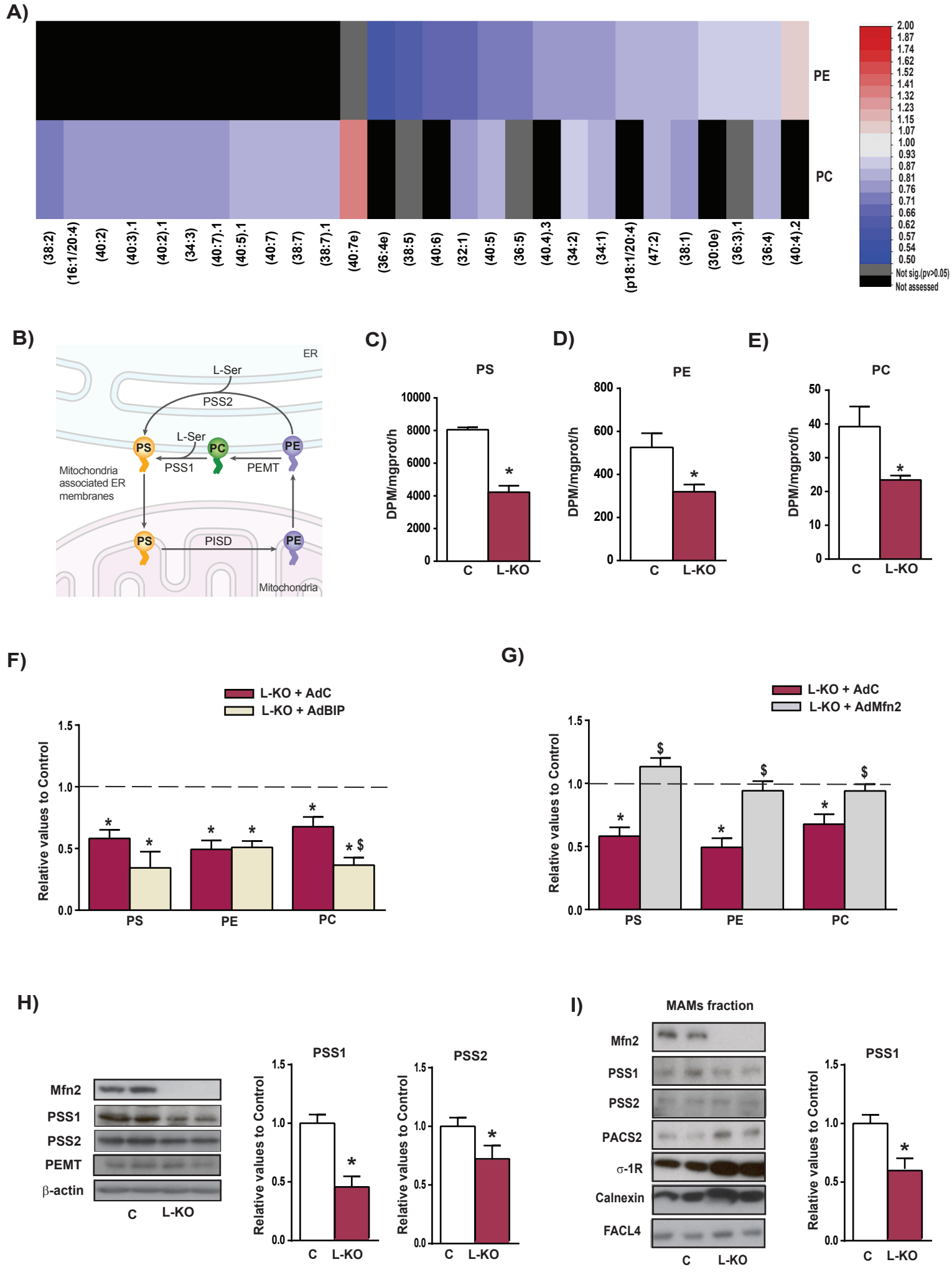
A)
PE
PC
2.00
1.87
1.74
1.62
1.52
1.41
1.32
1.23
1.15
1.07
1.00
0.93
0.87
0.81
0.76
0.71
0.66
0.62
0.57
0.54
0.50
Not sig.(pv>0.05)
Not assessed
(38:2)
(16:1/20:4)
(40:2)
(40:3).1
(40:2).1
(34:3)
(40:7).1
(40:5).1
(40:7)
(38:7)
(38:7).1
(40:7e)
(36:4e)
(38:5)
(40:6)
(32:1)
(40:5)
(36:5)
(40.4).3
(34:2)
(34:1)
(p18:1/20:4)
(47:2)
(38:1)
(30:0e)
(36:3).1
(36:4)
(40:4).2
B)
ER
L-Ser
PSS2
L-Ser
PS
PC
PE
PSS1
PEMT
Mitochondria associated ER membranes
PS
PISD
PE
Mitochondria
C)
PS
DPM/mgprot/h
10000
8000
6000
4000
2000
0
C
L-KO
D)
PE
DPM/mgprot/h
800
600
400
200
0
C
L-KO
E)
PC
DPM/mgprot/h
50
40
30
20
10
0
C
L-KO
F)
L-KO + AdC
L-KO + AdBIP
Relative values to Control
1.5
1.0
0.5
0.0
PS
PE
PC
G)
L-KO + AdC
L-KO + AdMfn2
Relative values to Control
1.5
1.0
0.5
0.0
PS
PE
PC
H)
Mfn2
PSS1
PSS2
PEMT
β-actin
C
L-KO
PSS1
Relative values to Control
1.5
1.0
0.5
0.0
C
L-KO
PSS2
Relative values to Control
1.5
1.0
0.5
0.0
C
L-KO
I)
MAMs fraction
Mfn2
PSS1
PSS2
PACS2
σ-1R
Calnexin
FACL4
C
L-KO
PSS1
Relative values to Control
1.5
1.0
0.5
0.0
C
L-KO

Figure 4

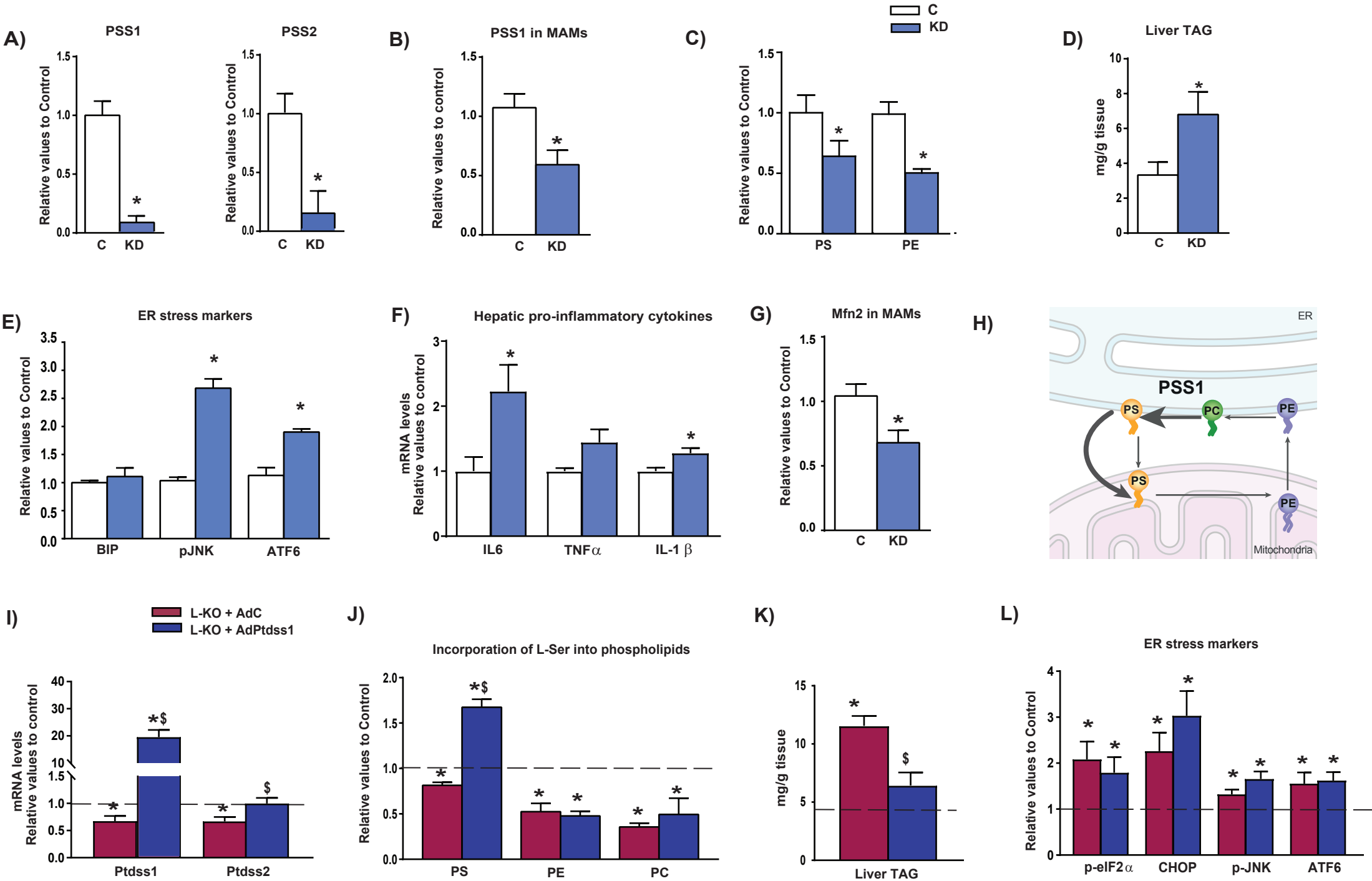
A)
PSS1
PSS2
Relative values to Control
C
KD
B)
PSS1 in MAMs
Relative values to control
C)
C
KD
PS
PE
D)
Liver TAG
mg/g tissue
E)
ER stress markers
BIP
pJNK
ATF6
F)
Hepatic pro-inflammatory cytokines
mRNA levels
Relative values to control
IL6
TNFα
IL-1 β
G)
Mfn2 in MAMs
H)
ER
PSS1
PS
PC
PE
Mitochondria
I)
L-KO + AdC
L-KO + AdPtdss1
Ptdss1
Ptdss2
J)
Incorporation of L-Ser into phospholipids
PS
PE
PC
K)
Liver TAG
L)
ER stress markers
p-eIF2α
CHOP
p-JNK
ATF6

Figure 5

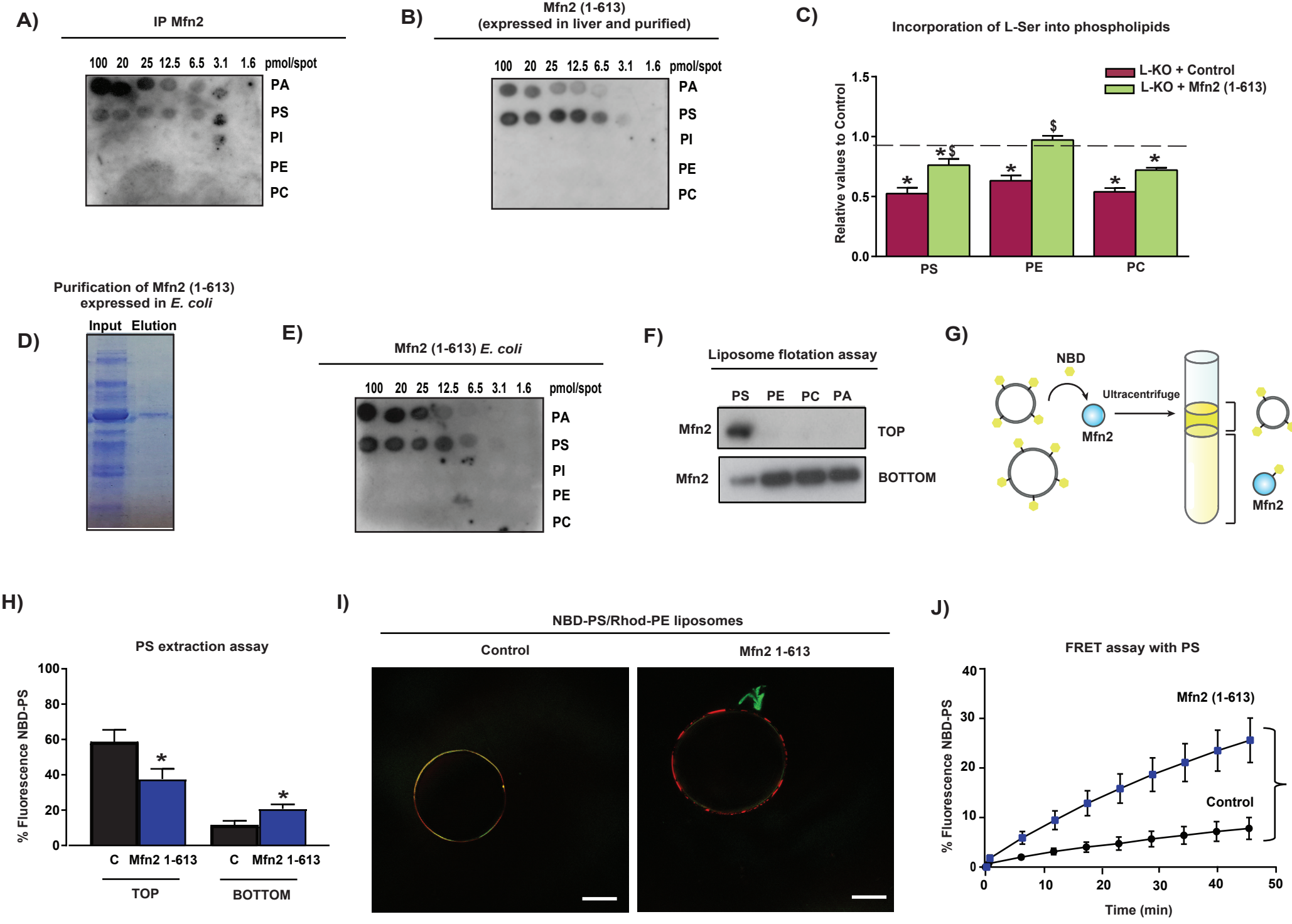
A)
IP Mfn2
100 20 25 12.5 6.5 3.1 1.6 pmol/spot
PA
PS
PI
PE
PC
B)
Mfn2 (1-613)
(expressed in liver and purified)
100 20 25 12.5 6.5 3.1 1.6 pmol/spot
PA
PS
PI
PE
PC
C)
Incorporation of L-Ser into phospholipids
L-KO + Control
L-KO + Mfn2 (1-613)
Relative values to Control
1.5
1.0
0.5
0.0
PS
PE
PC
Purification of Mfn2 (1-613)
expressed in E. coli
D)
Input Elution
E)
Mfn2 (1-613) E. coli
100 20 25 12.5 6.5 3.1 1.6 pmol/spot
PA
PS
PI
PE
PC
F)
Liposome flotation assay
PS PE PC PA
Mfn2
TOP
Mfn2
BOTTOM
G)
NBD
Ultracentrifuge
Mfn2
Mfn2
H)
PS extraction assay
% Fluorescence NBD-PS
100
80
60
40
20
0
C Mfn2 1-613 C Mfn2 1-613
TOP
BOTTOM
I)
NBD-PS/Rhod-PE liposomes
Control
Mfn2 1-613
J)
FRET assay with PS
% Fluorescence NBD-PS
40
30
20
10
0
Mfn2 (1-613)
Control
0 10 20 30 40 50
Time (min)

Figure 6

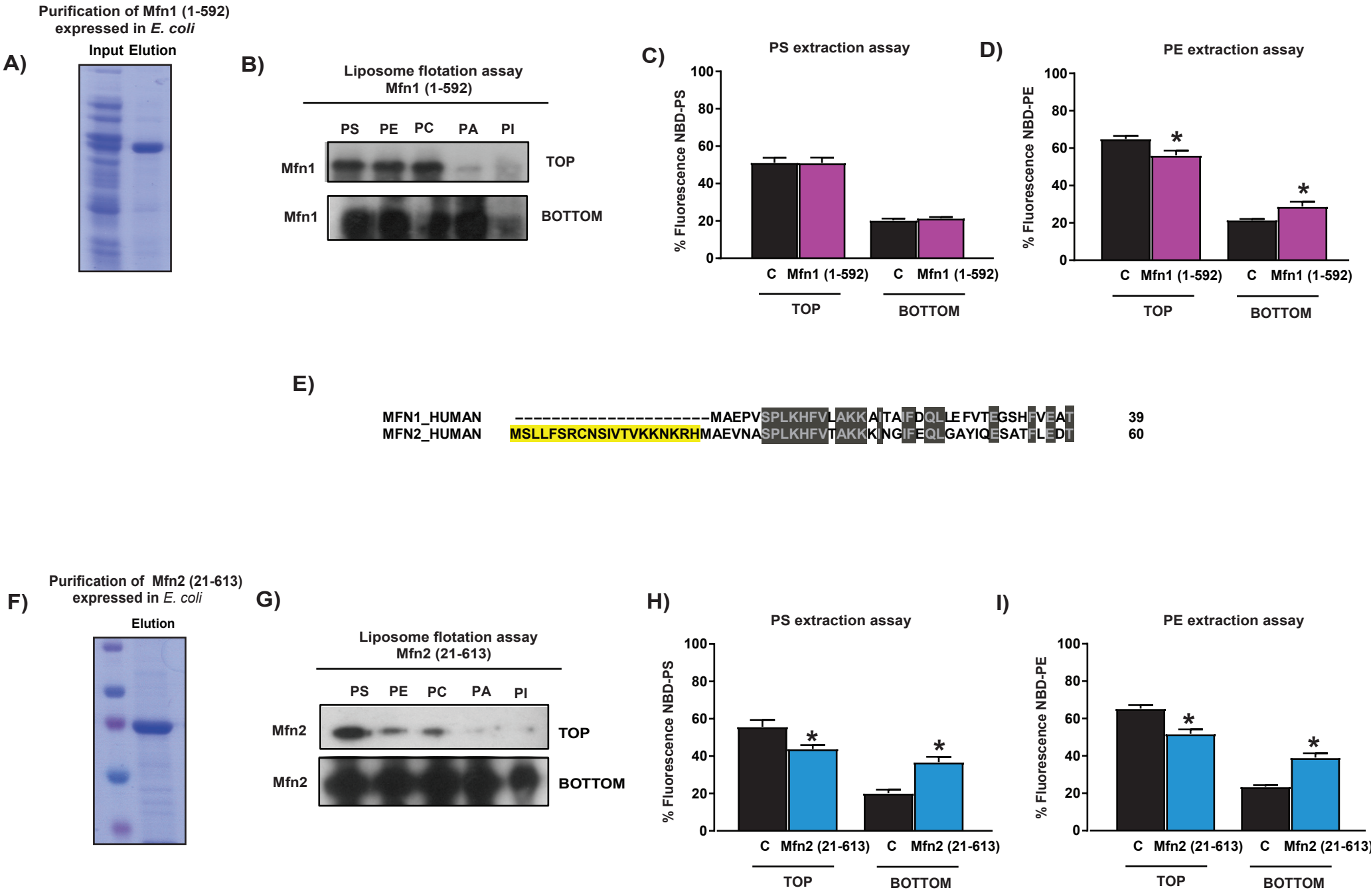
Purification of Mfn1 (1-592) expressed in E. coli
Input Elution
A)
B)
Liposome flotation assay
Mfn1 (1-592)
PS PE PC PA PI
Mfn1
TOP
Mfn1
BOTTOM
C)
PS extraction assay
% Fluorescence NBD-PS
100
80
60
40
20
0
C Mfn1 (1-592) C Mfn1 (1-592)
TOP
BOTTOM
D)
PE extraction assay
% Fluorescence NBD-PE
100
80
60
40
20
0
C Mfn1 (1-592) C Mfn1 (1-592)
TOP
BOTTOM
E)
MFN1_HUMAN ----------MAEPV
MFN2_HUMAN MSLLFSRCNSIVTVKKNKRHMAEVNA
39
60
F)
Purification of Mfn2 (21-613) expressed in E. coli
Elution
G)
Liposome flotation assay
Mfn2 (21-613)
PS PE PC PA PI
Mfn2
TOP
Mfn2
BOTTOM
H)
PS extraction assay
% Fluorescence NBD-PS
100
80
60
40
20
0
C Mfn2 (21-613) C Mfn2 (21-613)
TOP
BOTTOM
I)
PE extraction assay
% Fluorescence NBD-PE
100
80
60
40
20
0
C Mfn2 (21-613) C Mfn2 (21-613)
TOP
BOTTOM

Figure 7

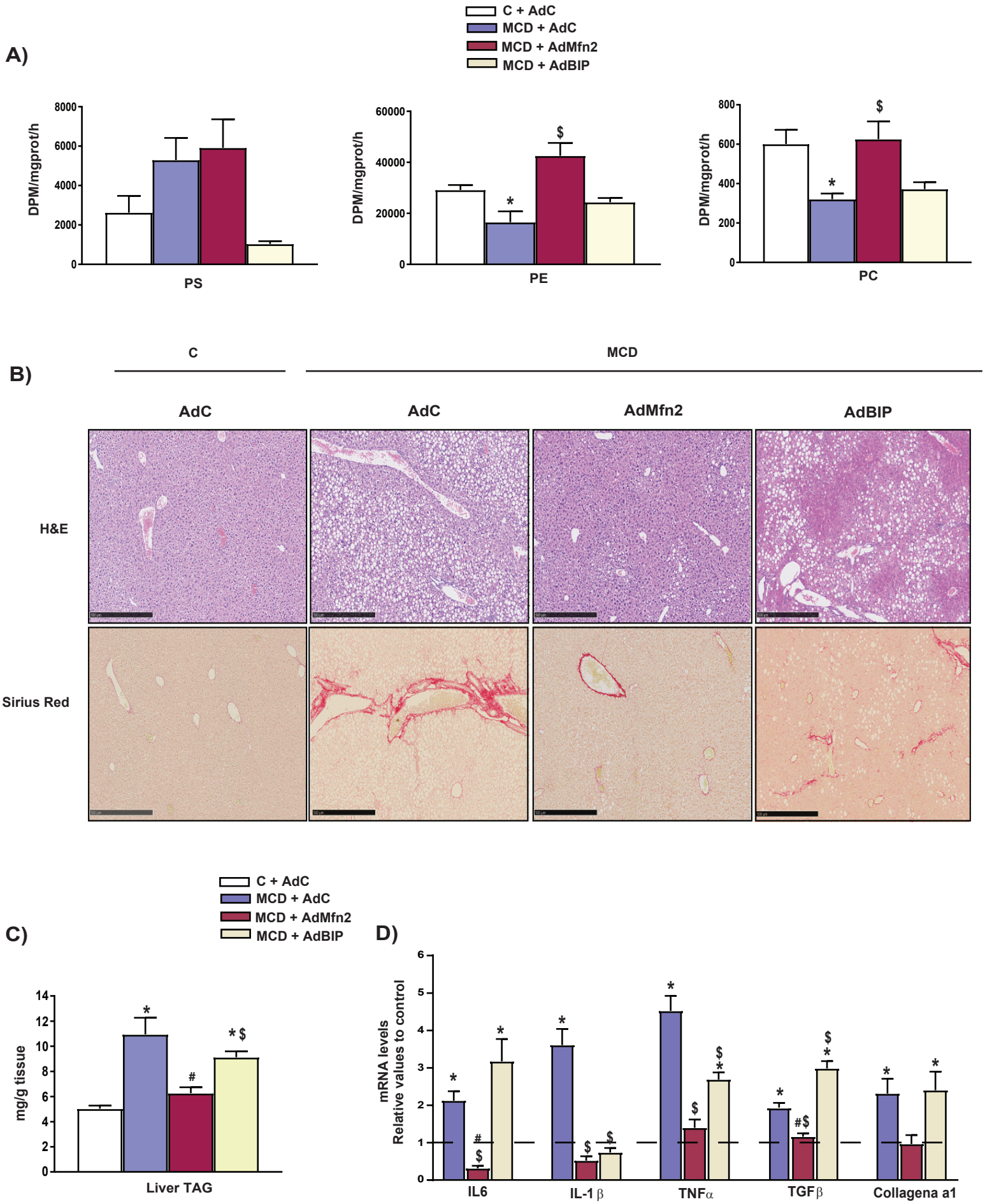
A)
C + AdC
MCD + AdC
MCD + AdMfn2
MCD + AdBIP
DPM/mgprot/h
PS
PE
PC
B)
C
MCD
AdC
AdC
AdMfn2
AdBIP
H&E
Sirius Red
C)
mg/g tissue
Liver TAG
D)
mRNA levels
Relative values to control
IL6
IL-1 β
TNFα
TGFβ
Collagena a1